Journal of Catalysis 435 (2024) 115541

Contents lists available at ScienceDirect

Journal of Catalysis

journal homepage: www.elsevier.com/locate/jcat

Research article

C—C bond cleavage in the electrooxidation of 2,3-butanediol controlled by an ionic liquid modifier

Juntao Yang [a], Florian Haßfurther [a], Felix Hilpert [a], Zarah Hussain [a], Tian Yang [a], Nicola Taccardi [b], Peter Wasserscheid [b,c], Olaf Brummel [a,*], Jörg Libuda [a]

[a] Interface Research and Catalysis, ECRC, Friedrich-Alexander-Universität Erlangen-Nürnberg, 91058 Erlangen, Germany
[b] Lehrstuhl für Chemische Reaktionstechnik, Friedrich-Alexander-Universität Erlangen-Nürnberg, 91058 Erlangen, Germany
[c] Forschungszentrum Jülich GmbH, Helmholtz-Institut Erlangen-Nürnberg for Renewable Energy, Germany

ARTICLE INFO

Keywords:
In-situ IR spectroscopy
Ionic liquids
Platinum
Secondary alcohols
Selectivity
Single crystals
Supported catalyst with ionic liquid layer

ABSTRACT

In heterogeneous catalysis, ionic liquids (ILs) are used as chemical modifiers to control selectivity. In our work, we aim to apply the same concept to electrocatalytic systems. As a model reaction, we studied the electrooxidation of 2,3-butanediol on the low-index Pt(1 1 1), Pt(1 0 0) and Pt(1 1 0) surfaces in an acidic environment. We used the IL 1-ethyl-3-methylimidazolium trifluoromethanesulfonate ($[C_2C_1Im][OTf]$) dissolved in an aqueous electrolyte as a catalyst modifier. The reaction mechanisms were investigated by electrochemical infrared reflection absorption spectroscopy (EC-IRRAS). The oxidation of 2,3-butanediol is highly structure dependent. On all three surfaces, the two products formed are acetoin and diacetyl, i.e. either one or two alcohol functionalities are oxidized. However, we observe distinct features on the different surfaces with respect to activity, potential window of oxidation, and selectivity. Only the Pt(1 0 0) surface is active towards C—C bond cleavage. The latter reaction leads to the formation of CO_{ads} and poisoning of the catalyst. Modification of this surface by addition of the IL leads to an increase of the selectivity for acetoin from 51 % to 78 % (at 1.1 V_{RHE}). In addition, C—C bond cleavage is suppressed, no CO is formed, and the surface remains active for the target reaction. We attribute these effects to the reversible and structure dependent adsorption of the $[OTf]^-$ anions on the Pt surfaces and additional interionic interactions. Our results demonstrate the potential of ILs to control selectivity in electrocatalytic reactions.

1. Introduction

Selectivity control is a major challenge in (electro)catalysis as it determines material and energy efficiency as well as purification costs [1]. In heterogeneous catalysis, a very successful approach to control selectivity is the modification of catalysts with ionic liquids (ILs, salts with melting points below 100 °C), known as "Solid Catalyst with Ionic Liquid Layer" (SCILL) [2–4]. In this approach, the surface of a porous catalyst is coated with a thin layer of IL. The interaction of the ionic liquid with the catalyst promotes selectivity through ligand effects, electronic modification of the catalyst, field effects, and blocking of unspecific sites [5–7]. Note, that the most unspecific sites are often the most active. Although this effect reduces the activity of the modified catalyst, it increases the selectivity. From an application point of view, the increase in selectivity is very often more relevant than the loss in activity. The success of the approach is demonstrated by the release of a SCILL for selective hydrogenation reactions on the industrial scale by Clariant AG [8].

In electrocatalysis, the use of ionic species (cations or anions) to affect the activity and selectivity is a known phenomenon. For example, Garcia et al. investigated the intrinsic cation effect ($Cs^+ > Na^+ > K^+ > Li^+$) on the OER activity of nickel oxyhydroxide (NiOOH) [9]. They proposed that bigger cations (Cs^+) interact with the Ni-OO^- species better, which leads to the stabilized $NiOO^-$-M^+ species, and consequently, a higher activity. Kamat et al. studied different anion effects on the ORR/OER activity. They observed that ORR activity follows the trend $HClO_4 > HNO_3 > H_2SO_4$ and OER activity follows the trend $HClO_4 > HNO_3 \sim H_2SO_4$. They attributed the effect to the different anion adsorption energies [10]. So et al. tuned the selectivity of the CO_2 reduction reaction (CO_2RR) on Cu by adding halides to the electrolyte [11]. They found that Cl^- and Br^- help to increase the CO selectivity. However, I^- leads to a decrease of the CO selectivity while it enhances

* Corresponding author.
E-mail address: olaf.brummel@fau.de (O. Brummel).

https://doi.org/10.1016/j.jcat.2024.115541
Received 6 February 2024; Received in revised form 21 April 2024; Accepted 6 May 2024
Available online 8 May 2024

the methane formation. They hypothesized that the selectivity effect is due to the halide adsorption on the Cu surface. In the case of I^-, CO protonation is favored by the induced negative charges.

By using ionic liquid modifiers, most of the attempts reported in the literature so far focus on increasing the activity in the conversion of small molecules [12–27]. In the pioneering work by Erlebacher et al. [22,23], they demonstrated increased activity for the oxygen reduction reaction (ORR) by modifying electrocatalysts with a hydrophobic IL. Besides ORR [14–17,22,23,27–31] improved activities have also been reported for other reactions such as the hydrogen oxidation reaction (HOR) [32], the oxygen evolution reaction (OER) [33,34], the hydrogen evolution reaction (HER) [35], and CO_2RR [18,36,37]. In addition, ILs can also improve the stability of the electrocatalyst [15,19,27,38,39].

The major advantages of modifying heterogeneous catalysts with ILs are, however, in the field of selectivity control. In electrocatalysis, this approach is still in its infancy [18,24,25]. Recently, we have shown that we can modify the Pt(1 1 1) electrode surface with the IL 1-ethyl-3-methyl-imidazolium trifluromethanesulfonate [C_2C_1Im][OTf] to control the selectivity in the oxidation of 2,3-butanediol [24]. The oxidation of 2,3-butanediol is of general interest because it is a model reaction for the oxidation of polyols with secondary alcohol functionalities [40–42]. Such reactions are of interest for the production of fine chemicals from renewable reactants [43]. For example, the reaction products of 2,3-butanediol oxidation, acetoin and diacetyl, are used as flavors in the food industry [44–46]. In addition, secondary alcohols have recently received lots of attention in the field of hydrogen storage. Here, secondary alcohols can serve as rechargeable electro-fuels, so called electrochemically active liquid organic hydrogen carriers (EC-LOHCs) [47–50].

In all these applications, however, selectivity is absolutely essential. In the case of EC-LOHCs, for example, C—C bond cleavage limits the cyclability of 2,3-butanediol in the oxidation/reduction cycle [51]. In this work, we compare the electrooxidation of 2,3-butanediol on the three most important Pt facets, i.e. Pt(1 1 1), Pt(1 0 0) and Pt(1 1 0). We demonstrate that electrooxidation of 2,3-butanediol is a highly structure sensitive reaction and we show that C—C bond cleavage takes place on the Pt(1 0 0) surface only. C—C bond cleavage results in the formation of CO and leads to poisoning of the surface. For Pt(1 1 1), we previously showed that we can modify the selectivity of 2,3-butanediol by adding a low concentration of the IL [C_2C_1Im][OTf] [24]. In this work, we demonstrate that, by adding the IL modifier, we not only change the selectivity towards the two products acetoin and diacetyl but we also suppress C—C bond cleavage on the Pt(1 0 0) surface. In this way, we can prevent the formation of the catalyst poison CO.

2. Experimental

2.1. Cleaning procedure

To avoid contamination, we cleaned all glass and Teflon parts as well as noble metal wires with a dedicated cleaning procedure. We soaked all Teflon and glass parts overnight in a solution of NOCHROMIX (Sigma-Aldrich) in concentrated H_2SO_4 (Merck, EMSURE, 98 %) and rinsed the equipment afterwards five times with ultrapure water (Milli-Q Synergy UV, 18.2 MΩ cm at 25 °C, TOC < 5 ppb). This was followed by three cycles of boiling and rinsing with ultrapure water. We annealed all noble metal wires in the flame of a Bunsen burner and rinsed the wires afterwards with ultrapure water.

2.2. Preparation of Pt(h k l) electrodes and solutions

We used Pt(h k l) single crystals from MaTecK (99.999 %, depth of roughness < 0.01 μm, accuracy of orientation < 0.4°) for IR spectroscopy or Pt(1 1 1) from icryst (depth of roughness < 0.05 μm, accuracy of orientation < 0.5°, surface area 4.5 mm^2) or Pt(1 0 0) and Pt(1 1 0) from SPL (depth of roughness < 0.03 μm, accuracy of orientation < 0.1°, surface arear 6.6 mm^2) for cyclic voltammetry. We annealed the single crystals in the blue flame of a Bunsen burner for 2 min. Subsequently, we cooled the single crystals in Ar/H_2 (Linde 5.0; volume ratio of ~3:1) atmosphere to room temperature. For the transfer to the electrochemical cells, we protected the surface of the single crystals with a droplet of ultrapure water. We prepared solutions of 2,3-butanediol (Sigma Aldrich 98 %) and $HClO_4$ (Merck, Suprapur or Carl Roth, Ultra 70 %). To ensure highest purity, the IL [C_2C_1Im][OTf] was synthesized and purified in-house according to a previously described procedure [52]. We purchased lithium trifluoromethanesulfonate from Merck with a purity of 99.995 %. We degassed all solutions by purging with Ar (Linde, 5.0) for at least 20 min.

2.3. CV measurement

We recorded CVs with 50 mVs^{-1} in hanging meniscus configuration using a three-electrode setup and a commercial potentiostat (Gamry Reference 600+). We used a Pt wire as the counter electrode (CE) and a home-built reversible hydrogen electrode (RHE) as the reference electrode (RE). Before the measurements, we confirmed the cleanliness of the cells by performing a CV of Pt(1 1 1) in 0.1 M $HClO_4$ solution. All electrolytes were thoroughly purged by N_2 for at least 20 min before recording CVs. The volume of the CV cell that was filled with gas was continuously purged with N_2.

2.4. EC-IRRAS

For the electrochemical infrared reflection absorption spectroscopy (EC-IRRAS) measurements, we used a commercial IR spectrometer with evacuated optics (Bruker Vertex 80v) and a liquid nitrogen cooled mercury cadmium telluride (MCT) narrow band detector. The spectrometer was equipped with commercial optics for electrochemical measurements, a home-built electrochemical cell, and a motorized polarizer. We used a CaF_2 hemisphere (Korth) as IR transparent window material sealed with a Kalrez gasket. We controlled the potential by a commercial potentiostat (Gamry Reference 600). We used a Pt wire as CE and a home-built RHE as RE. We recorded reference spectra (256 scans per spectrum) in p- and s-polarization at 0.05 V_{RHE} before each measurement. We recorded IR spectra with 128 scans per spectrum, a resolution of 2 cm^{-1} and an acquisition time of 51.5 s per spectrum between 0.05 and 1.1 V_{RHE}. The spectra were measured with p- and s-polarized light at each potential step. A more detailed description of the IR setup used, we provide in literature [53].

3. Results and discussion

In this work, we studied the oxidation of 2,3-butanediol, by EC-IRRAS (see Scheme 1). The electrooxidation of 2,3-butanediol occurs in two steps, releasing four protons and four electrons after complete oxidation (Scheme 1a). In a first two-electron process, 2,3-butanediol is oxidized to the partially oxidized intermediate acetoin. In a second two-electron process, acetoin is further oxidized to the fully oxidized diacetyl [42]. We studied the reaction on low-index Pt(h k l) single crystal electrodes, namely Pt(1 1 1), Pt(1 0 0) and Pt(1 1 0) (Scheme 1b) prepared by flame annealing [54]. This preparation procedure results in well-ordered surfaces [55]. Representative cyclic voltammograms (CVs) of these surfaces are provided in the Supporting Information (Figs. S1 and S2). To modify the electrodes, we used the IL [C_2C_1Im][OTf] (Scheme 1c). Note, that the $[OTf]^-$ anion of this IL adsorbs on platinum surfaces in the potential range of interest in a potential-dependent and reversible manner [52].

First, we studied the electrooxidation of 2,3-butanediol on Pt(h k l) single crystal electrodes by measuring cyclic voltammetry (CV), which we provide in the Supporting Information (Fig. S2). The observation of different CV profiles indicates that the oxidation reaction is highly surface sensitive. To investigate the origin of the oxidation peaks in the CVs,

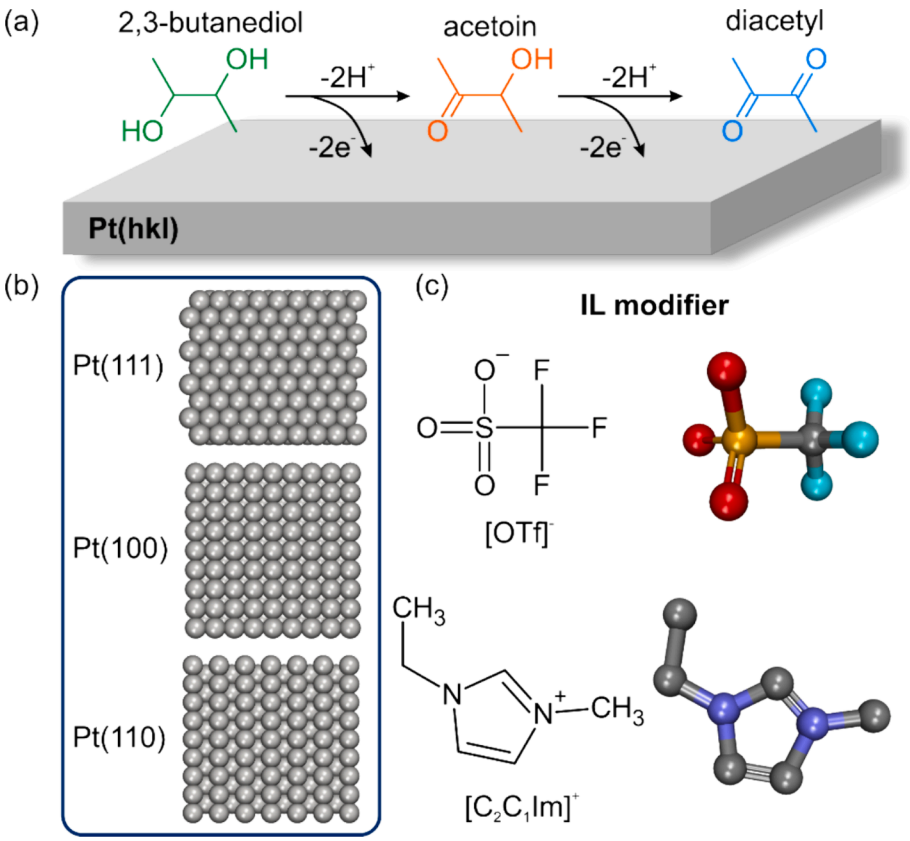

Scheme 1. Electrooxidation of 2,3-butanediol on Pt(h k l) electrodes in the absence and in the presence of the IL modifier $[C_2C_1Im][OTf]$; (a) schematic representation of the reaction; (b) models of the Pt(1 1 1), Pt(1 0 0) and Pt(1 1 0) surfaces; (c) molecular structure of the IL modifier $[C_2C_1Im][OTf]$.

we performed in-situ EC-IRRAS.

In a first step, we recorded the IR spectra of 2,3-butanediol, acetoin and diacetyl by attenuated total reflection (ATR) IR spectroscopy (Fig. 1a) and assigned the IR bands to the corresponding vibrational modes (Table 1), based on the DFT calculations reported in our previous work [24]. To identify the species in the in-situ experiment, we used the intense ν(C═O) band which is characteristic for ketones. However, this band does not allow differentiation between the ketones acetoin and diacetyl. Therefore, we used in addition the band at 1200 cm^{-1} (ν(CC)) which is specific for acetoin. Note that for quantification we also used the bands at 1358 cm^{-1} (ν_{as}(CC)/$\delta(CH_3)$, diacetyl) and 1380 cm^{-1} (δ(CCH)/$\delta(CH_3)$, 2,3-butanediol).

In the next step, we studied the electrooxidation of 2,3-butanediol in-situ on Pt(1 1 1), Pt(1 0 0), and Pt(1 1 0) single crystal electrodes in the absence of IL by EC-IRRAS. We used a solution of 0.2 M 2,3-butanediol in 0.1 M $HClO_4$. Reference spectra were recorded at 0.05 V_{RHE}. The potential was then increased in 0.1 V steps from 0.05 to 1.1 V_{RHE}. We recorded spectra in p- and in s-polarization at each potential step. Note that this procedure allows us to distinguish between adsorbed species and species in solution by comparing the spectra measured with different polarization. While the spectra measured in p-polarization contain information about adsorbed species and the species in solution, the spectra measured in s-polarization contain information about species in solution only due to the metal surface selection rule (MSSR) [56]. EC-IRRA spectra recorded with p-polarized light are shown in Fig. 1. All spectra are difference spectra with respect to the reference spectrum. Therefore, positive bands (peaks pointing upwards) indicate consumed species and negative bands (peaks pointing downwards) indicate formed species. For all surfaces, we observe positive bands in the IR fingerprint region at 1457 cm^{-1} and negative bands at 1717, 1361 and 1200 cm^{-1}. The band intensity increases with increasing potential. We observe only minor differences in the onset potentials for oxidation, with an onset of 0.4 V_{RHE} for Pt(1 1 1) and Pt(1 0 0) and 0.5 V_{RHE} for Pt(1 1 0). Distinct differences are observed in the development of the band at 1200 cm^{-1}, which is the spectroscopic marker for acetoin (see above). On Pt(1 1 1), this band reaches a maximum at 0.6 V_{RHE} and decreases subsequently. On the other surfaces this decrease is much weaker. In sharp contrast to the results on Pt(1 1 1) and Pt(1 1 0), we observe two pronounced negative bands at 2020 and 1819 cm^{-1} on Pt(1 0 0) above 0.4 V_{RHE}, i.e. in the frequency region of adsorbed CO. The CO features on Pt(1 0 0) show characteristic blue shifts (68 cm^{-1} V^{-1} for CO_t and 75 cm^{-1} V^{-1} for CO_b) with increasing potential. Above 0.8 V_{RHE} these bands disappear and a new band is observed at 2343 cm^{-1} (onset ~ 0.6 V_{RHE}). The latter band has been assigned to the asymmetric stretching mode ν_{as}(OCO) of CO_2 [52]. The CO_2 band is much stronger on the Pt(1 0 0) surface as compared to the two other surfaces where this band is extremely weak.

The positive band at 1457 cm^{-1} is attributed to the $\delta(CH_3)$ mode of 2,3-butanediol, indicating the consumption of 2,3-butanediol with an onset at 0.4/0.5 V_{RHE}, depending on the surface structure. The negative bands at 1717, 1361 and 1200 cm^{-1} are in good agreement with the reference spectra of the two products acetoin and diacetyl and are assigned to the ν(C═O) mode, the ν_{as}(CC)/$\delta(CH_3)$ mode and the ν(CC) mode, respectively. These bands indicate the formation of acetoin and diacetyl. On Pt(1 1 1), the development of the band at 1200 cm^{-1}, which is characteristic for acetoin, indicates that acetoin is formed in a first oxidation step. The acetoin reacts further to diacetyl as indicated by the decrease of this band at higher potential. This is in perfect agreement with previous observations [24]. On Pt(1 0 0) and Pt(1 1 0), however, the decrease in intensity of the band at 1200 cm^{-1} is much less pronounced. At this stage, there would be two explanations to this phenomenon: On the one hand, it is possible that the second oxidation step to diacetyl is suppressed on these surfaces. On the other hand, it is also possible that the formation of acetoin and reaction to diacetyl occur in parallel. We will return to this point when we discuss the quantitative analysis of this

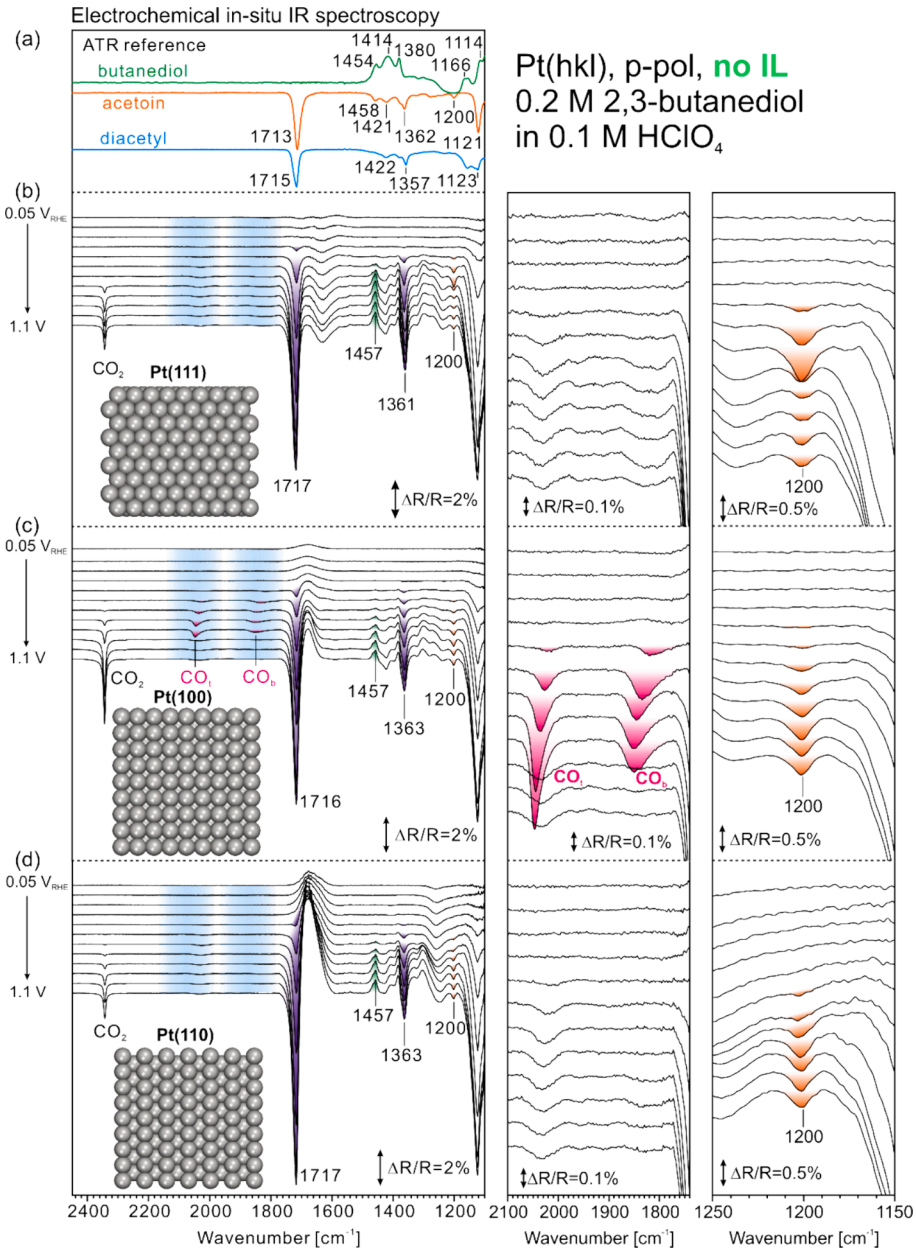

Fig. 1. Electrochemical in-situ IR spectra recorded during the oxidation of 2,3-butanediol on low-index Pt surfaces; (a) ATR IR spectra of the reactant 2,3-butanediol (green) and the products acetoin (orange) and diacetyl (blue); in-situ IR spectra recorded on (b) Pt(1 1 1), (c) Pt(1 0 0) and (d) Pt(1 1 0) in p-polarization with enlarged sections of the CO region (indicated in the overview in blue) and the region of the spectroscopic marker for acetoin at 1200 cm^{-1}; 0.2 M 2,3-butanediol in 0.1 M $HClO_4$; reference spectra were recorded at 0.05 V_{RHE}. (For interpretation of the references to colour in this figure legend, the reader is referred to the web version of this article.)

experiment.

On Pt(1 0 0), we assign the two negative bands at 2020 and 1819 cm^{-1}, observable only in p-polarization, to the formation of CO adsorbed in on-top (CO_t) and bridge-bonded (CO_b) geometry, respectively [57,58]. The potential dependent frequency shift of 27 cm^{-1} (CO_t) and 30 cm^{-1} (CO_b) results from the Stark effect [56] and an increased dipole coupling due to increased CO coverage [59]. The values fit very well to the values reported in literature [56]. In sharp contrast, all signals in the spectrum of Pt(1 1 1) are also observable in s-polarization, ruling out the presence of CO (see Fig. S3 in the Supporting Information). For Pt(1 1 0), there are very small differences between the CO-region in p- and s-polarization, suggesting that there might be traces of CO formed on Pt (1 1 0), but the amount is extremely small. The observations clearly indicate that the Pt(1 0 0) surface is active towards CO formation during the electrooxidation of 2,3-butanediol. This finding is in perfect agreement with previous work by Feliu et al., who observed a similar structure dependence for the simpler secondary alcohol isopropanol [51]. The formation of CO_{ads} on Pt(1 0 0) implies that the Pt(1 0 0) surface is active towards C—C bond cleavage during the electrooxidation of 2,3-butanediol. Often, electrocatalytic reactions, especially those involving bond cleavage, take place preferentially on (1 0 0) surfaces, such as alcohol/ammonia oxidation on Pt [51,60], CO reduction on Cu [61,62], oxygen reduction on Au [63]. By studying the irreversible adsorption of ethyl pyruvate on Pt(h k l) single crystals, Hazzazi et al. concluded that the decomposition of ethyl pyruvate is favored on Pt(1 0 0), yielding adsorbed CO, which requires a special geometry or number of free Pt sites [64]. This is also supported by the study of Bondue et al. [65] who suggested that the dissociative adsorption of acetone on Pt only occurs at

Table 1
Band assignments and vibrational modes of 2,3-butanediol, acetoin and diacetyl. (Meso: *meso*-2,3-butandediol; SS: 2S,3S-butanediol; RR: 2R,3R-butanediol).

2,3-butanediol		Acetoin		Diacetyl	
ν [cm^{-1}]	vibrational modes [24]	ν [cm^{-1}]	vibrational modes [24]	ν [cm^{-1}]	vibrational modes [24]
1114	ν_{as}(C—C—OH) (meso) ν(CC), ν(CC) (SS/RR)	1121	ν (COH)	1123	ν_{as}(CC)
1166	ν (CC)	1200	ν (CC)	1357	ν_{as}(CC)/ δ(CH3)
1380	δ(CCH), δ(CCH) (meso), δ(COH) (SS/RR)	1362	ν (CC)	1422	$\delta(CH_3)$
1414	ν(CC), ν(CC), δ(COH), ν(CC) (meso) $\delta(CH_3)$, $\delta(CH_3)$, $\delta_{sym}(CH_3)$, ν(CC) (SS/RR)	1421	$\delta(CH_3)$	1715	ν_{as}(C=O)
1454	$\delta(CH_3)$ (meso) $\delta(CH_3)$ (SS/RR)	1458 1713	$\delta(CH_3)$ ν (C=O)		

the (1 0 0) terrace sites with an 'ensemble' of free Pt atoms. Using DFT calculations, Li et al. studied in detail the structural preference for bond-making and breaking reactions on (1 0 0) terrace sites [66,67]. They attributed the effects observed to an ensemble of several surface atoms on the (1 0 0) terrace. Our result is in good agreement with the above mentioned experimental and computational studies. Therefore, we would expect that the C—C bond cleavage on Pt(1 0 0) in the electro-oxidation of 2,3-butanediol also requires a special ensemble site, which includes a minimum number of free surface Pt atoms and is only possible on Pt(1 0 0) terraces.

In Fig. 1, the band at 2343 cm^{-1} is assigned to the ν_{as}(OCO) band of CO_2. The distinct differences in the band intensities indicate that CO_2 is formed preferentially on the Pt(1 0 0) surface. As this surface is active towards C—C bond cleavage and CO formation, we propose that CO_2 is, at least in part, formed by electrooxidation of CO_{ads}. On the other surfaces, the band intensity of CO_2 is very low and comparable to CO_2 formed during the oxidation of isopropanol on Pt(1 1 1) and Pt(1 1 0) [51,68]. Feliu et al. proposed that the traces of CO_2 observed on Pt(1 1 1) and Pt(1 1 0) may originate from defect sites, which are always present on the large single crystals used for IR spectroscopy [51].

In the next step, we compare the spectra measured in p- and in s-polarization in more detail. The comparison for the Pt(1 0 0) surface is shown in Fig. 2 (see Fig. S4 in the Supporting Information for the other surfaces). First, we note that the bands associated with CO_t and CO_b are visible in p-polarization only. Secondly, the negative bands at ~1714, 1363, and 1200 cm^{-1} assigned to the products acetoin and diacetyl are much more intense in p-polarization than in s-polarization. In addition, there is a small blue shift in p-polarization as compared to s-polarization (note that the spectra in polarizations were measured in the same experiment). The presence of the CO_{ads} bands in p-polarization confirms that the CO species are adsorbed on the Pt surface. For the two products acetoin and diacetyl, we observe a lower band intensity in s-polarization. Additionally, we observe a shift of the peak position of the carbonyl band. Taking into account the MSSR, we conclude that the products remain partially adsorbed on the Pt(1 0 0) surface. We have previously observed similar behavior for isopropanol oxidation [68–70].

Next, we quantitatively analyzed the IR spectra measured in s-polarization (solution only) using the Beer-Lambert law. After determining the thin layer thickness and the extinction coefficients of selected IR bands, we calculated the concentration changes of 2,3-butanediol, acetoin and diacetyl as a function of potential. We then determined the selectivity of acetoin by the equation: $Selectivity_{acetoin} = C_{acetoin}/(C_{acetoin} + C_{diacetyl})$. For detailed information, we refer to our previous work [24]. Note that the selectivity might also depend on the applied experimental protocol and, at this point, we will discuss the selectivity for our specific experiment only, in which we increased stepwise the potential and we accumulate the products over the applied protocol. All results of the quantitative analysis are summarized in Fig. 3. The initial concentration of the reactant 2,3-butanediol was 0.2 M. Distinct differences are observed with respect to the potential-dependent evolution of the different species, and the selectivity.

On Pt(1 1 1), the conversion occurs in a potential window between

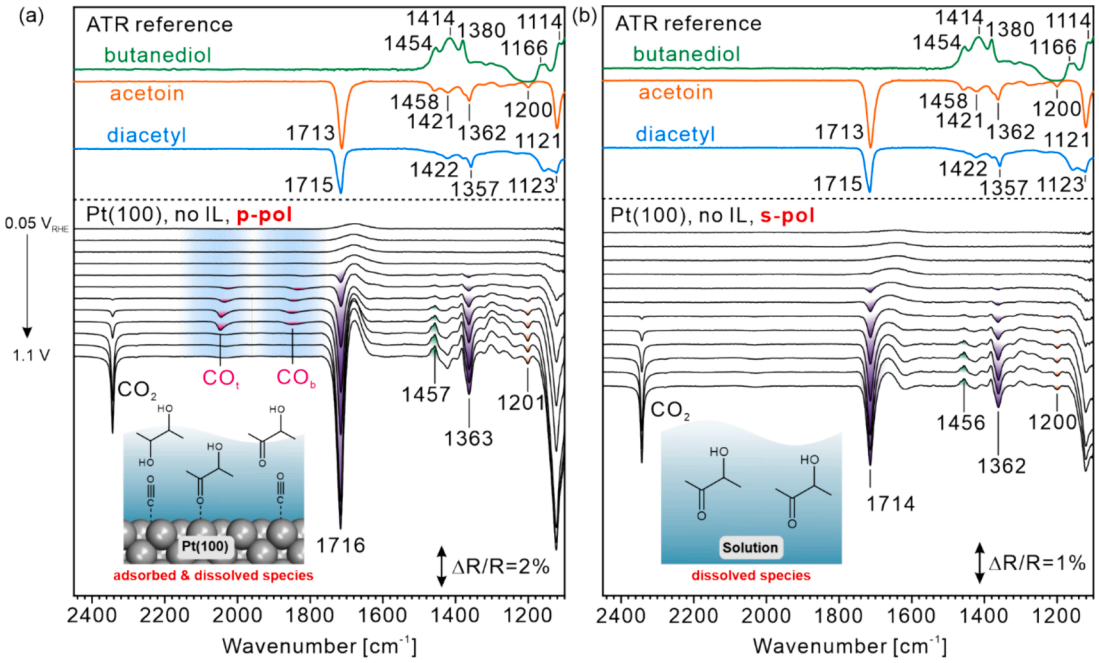

Fig. 2. Comparison of the electrochemical in-situ IR spectra on Pt(1 0 0) recorded with (a) p- and (b) s-polarized light during the oxidation of 2,3-butanediol; 0.2 M 2,3-butanediol in 0.1 M $HClO_4$; reference spectra were recorded at 0.05 V_{RHE}; the spectral region of the CO_t and CO_b adsorbed on Pt is highlighted in blue. (For interpretation of the references to colour in this figure legend, the reader is referred to the web version of this article.)

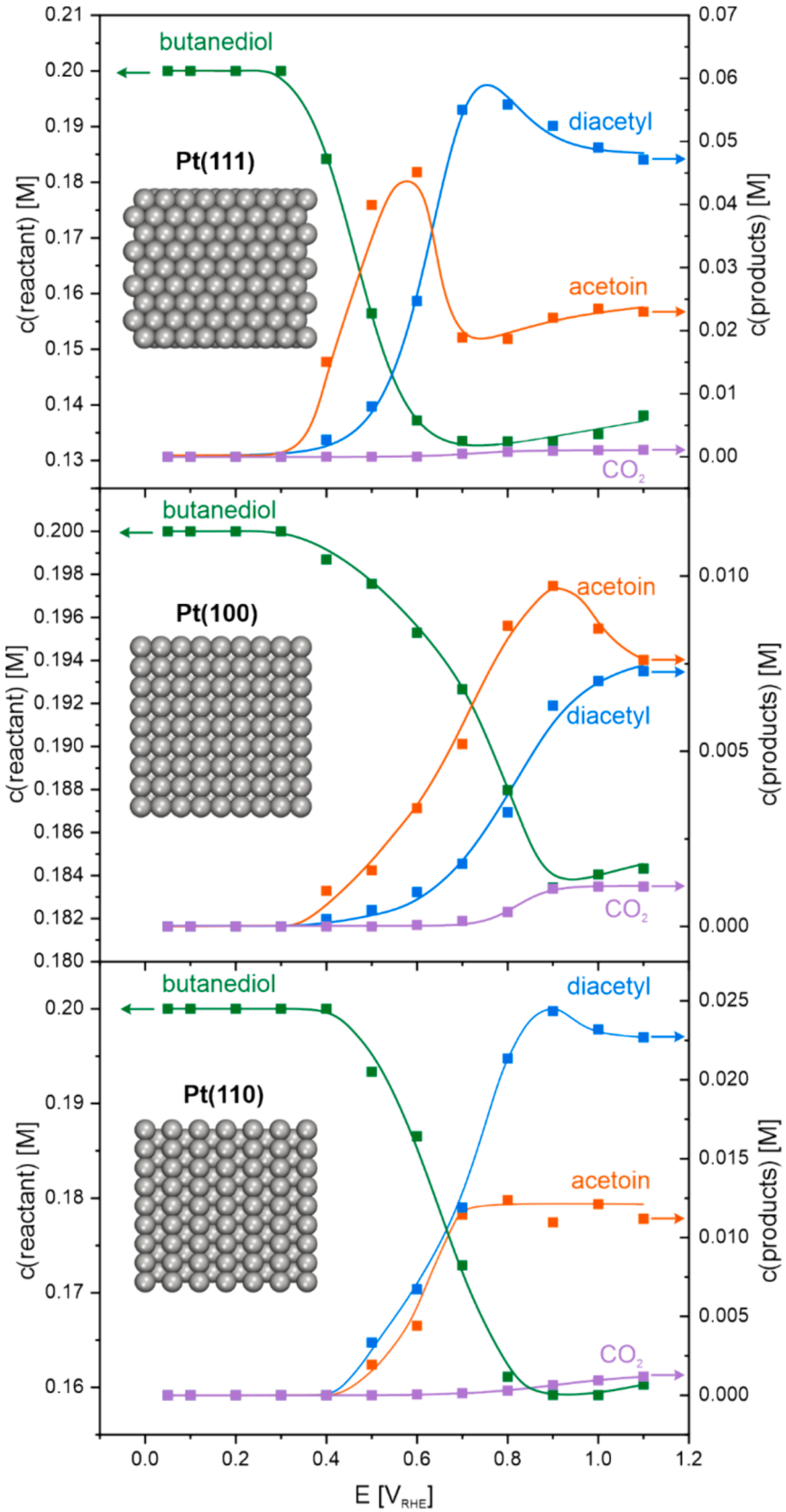

Fig. 3. Potential dependent development of the concentrations of 2,3-butanediol (green), acetoin (orange), diacetyl (blue) and CO_2 (purple) on Pt(1 1 1) (top), Pt (1 0 0) (middle), and Pt(1 1 0) (bottom) during the oxidation of 2,3-butanediol determined from IR spectra measured with s-polarized light; 0.2 M 2,3-butanediol in 0.1 M $HClO_4$. (For interpretation of the references to colour in this figure legend, the reader is referred to the web version of this article.)

0.4 and 0.7 V_{RHE}. At low potentials, acetoin is preferentially formed. The concentration of acetoin reaches a maximum of ~45 mM at 0.6 V_{RHE} and decreases rapidly to ~20 mM at higher potentials. Above 0.6 V_{RHE}, diacetyl becomes the dominant species and reaches a concentration of 55 mM. At potentials of 0.7 V_{RHE} and above, the formation of both diacetyl and acetoin levels off and we detect the formation of very small concentrations of CO_2 (<1.5 mM) only.

On Pt(1 0 0), the onset potential is also 0.4 V_{RHE} but the potential window for conversion is much broader (0.4–1.1 V_{RHE}). At low potential, acetoin is formed preferentially and a peak in the acetoin concentration is observed at 0.9 V_{RHE}. We note that this peak occurs at much higher potentials as compared to Pt(1 1 1) and the following decrease in acetoin concentration is less pronounced. Furthermore, there is a larger overlap between the potential windows for acetoin and diacetyl formation. At 1.1 V_{RHE}, the diacetyl and acetoin concentrations reach a value of ~7.5 mM.

On the Pt(1 1 0) surface, the on-set of the 2,3-butanediol oxidation is shifted by 0.1 V to higher potentials (0.5 V_{RHE}) and acetoin and diacetyl formation occur in parallel. At 0.7 V_{RHE}, the concentration of acetoin levels off at a concentration of 12 mM. In contrast to Pt(1 1 1), we observe, however, no significant decrease in acetoin concentration at potentials above 0.7 V_{RHE}. Diacetyl is formed up to 0.9 V_{RHE}, reaching a concentration of ~25 mM, while 2,3-butanediol is consumed. Above 0.7 V_{RHE}, low amounts of CO_2 are formed (1.2 mM). At 1.1 V_{RHE}, the selectivities of acetoin are 33 %, 51 %, and 31 % for Pt(1 1 1), Pt(1 0 0), and Pt(1 1 0), respectively.

In summary, all surfaces are active towards the formation of the partially oxidized acetoin and the fully oxidized diacetyl. However, the selectivities, activities, and potential windows differ. On Pt(1 1 1) acetoin is formed as an intermediate which is oxidized to diacetyl at higher potential. On Pt(1 0 0) and Pt(1 1 0), the formation of acetoin and diacetyl occurs in the same potential window. C—C bond cleavage and CO_{ads} formation occurs on Pt(1 0 0) only. We attribute the much lower activity of Pt(1 0 0) and the shifted maxima of the oxidation steps to poisoning by CO_{ads}, formed as a result of C—C bond cleavage.

Once, we have studied the oxidation of 2,3-butanediol on non-modified Pt(h k l) surfaces, in the next step, we investigated the effect of the IL [C_2C_1Im][OTf] on the selectivity. The experimental procedure was identical to the experiments without IL. In particular, we focus on the C—C bond cleavage, which occurs on the Pt(1 0 0) surface. First we performed CV measurements in the presence of the IL on Pt(1 0 0) (see Fig. S5 in the Supporting Information). We observe a decrease of the oxidation peak in the presence of the IL. In Fig. 4, we compare the IR spectra recorded in p-polarization in the absence and in the presence of different concentrations of the IL. We observe the same bands of butanediol, acetoin, and diacetyl, however, with distinct differences in the onset potential, peak intensity, and intensity ratio. In general, the onset potentials increase with increasing IL concentration (up to 0.7 V_{RHE} at 10 mM IL) as compared to the situation without IL (Fig. 4b–d). Secondly, we observe a decrease in band intensity with increasing IL concentration. However, the most significant differences were observed in the CO_{ads} bands. Already at the very low IL concentrations of 1 mM (Fig. 4c), the CO_{ads} band intensity decreases drastically. At a concentration of 10 mM IL, the CO_{ads} bands disappear completely (Fig. 4d). Note, that we still observe the bands of the products acetoin and diacetyl, indicating that the Pt(1 0 0) surface is still active for product formation. The absence of any CO_{ads} on the surface indicates that the reaction channel of C—C bond cleavage leading to the formation of CO is completely suppressed. To study whether or not the anion alone is the modifier that suppresses the poisoning species, we performed the same experiment except using the salt with different cation, i.e. Li[OTf]. As shown in the Fig. S6 (Supporting Information), we still observe the bands of CO_t and CO_b in the presence of 10 mM Li[OTf] with similar intensity as in the control experiment in the absence of the salt. Therefore, we conclude that not only the adsorption of the anion but also additional interionic interactions are required to suppress the formation of the poisoning

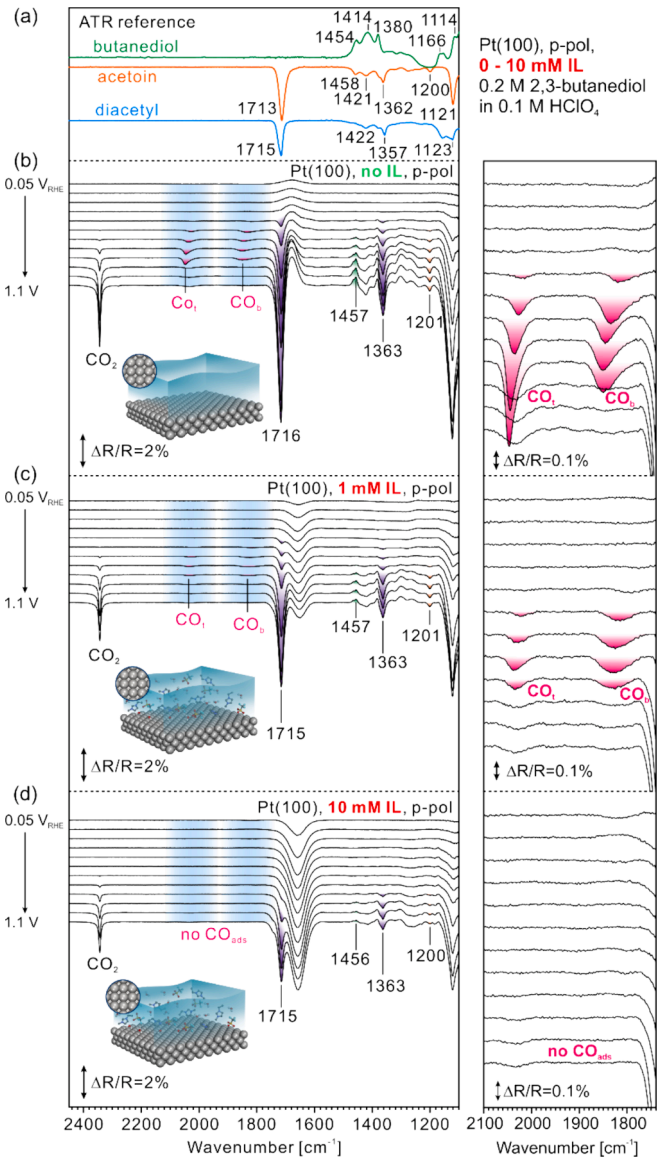

Fig. 4. Electrochemical in-situ IR spectra recorded with p-polarized light during the oxidation of 2,3-butanediol on Pt(1 0 0) in the absence and presence of the IL [C_2C_1Im][OTf]; (a) ATR IR spectra of 2,3-butanediol (green), acetoin (orange) and diacetyl (blue); in-situ IR spectra recorded in the (b) absence and (c) presence of 1 mM and (d) 10 mM of IL; 0.2 M 2,3-butanediol in 0.1 M $HClO_4$; reference spectra were recorded at 0.05 V_{RHE}. (For interpretation of the references to colour in this figure legend, the reader is referred to the web version of this article.)

species CO. Successively, we quantitatively analyzed the in-situ IR spectra recorded in s-polarization in the absence (Fig. 5a) and presence (1 mM, Fig. 5b) of IL (see spectra in Supporting Information, Fig. S7). Besides the direct effect on the on-set potential discussed above, we observe differences in the overall conversion and in the distribution of the formed products (note, that a quantitative analysis of the spectra measured in 10 mM IL is challenging due to the low signal intensity of the products caused by the lower activity). The total conversion of butanediol decreases from 10 % to 4 % in the presence of 1 mM IL. In the absence of IL, the acetoin concentration reaches a maximum at 10 mM and decreases slightly at higher potentials. Diacetyl is formed up to a potential of 1.0 V_{RHE}, reaching a selectivity for acetoin of 51 % at 1.1 V_{RHE} (see Fig. 5c). In the presence of the IL, diacetyl is formed below 0.9 V_{RHE} and the reaction stops at higher potentials. This results in a much higher selectivity towards acetoin of 78 % at 1.1 V_{RHE} (Fig. 5c).

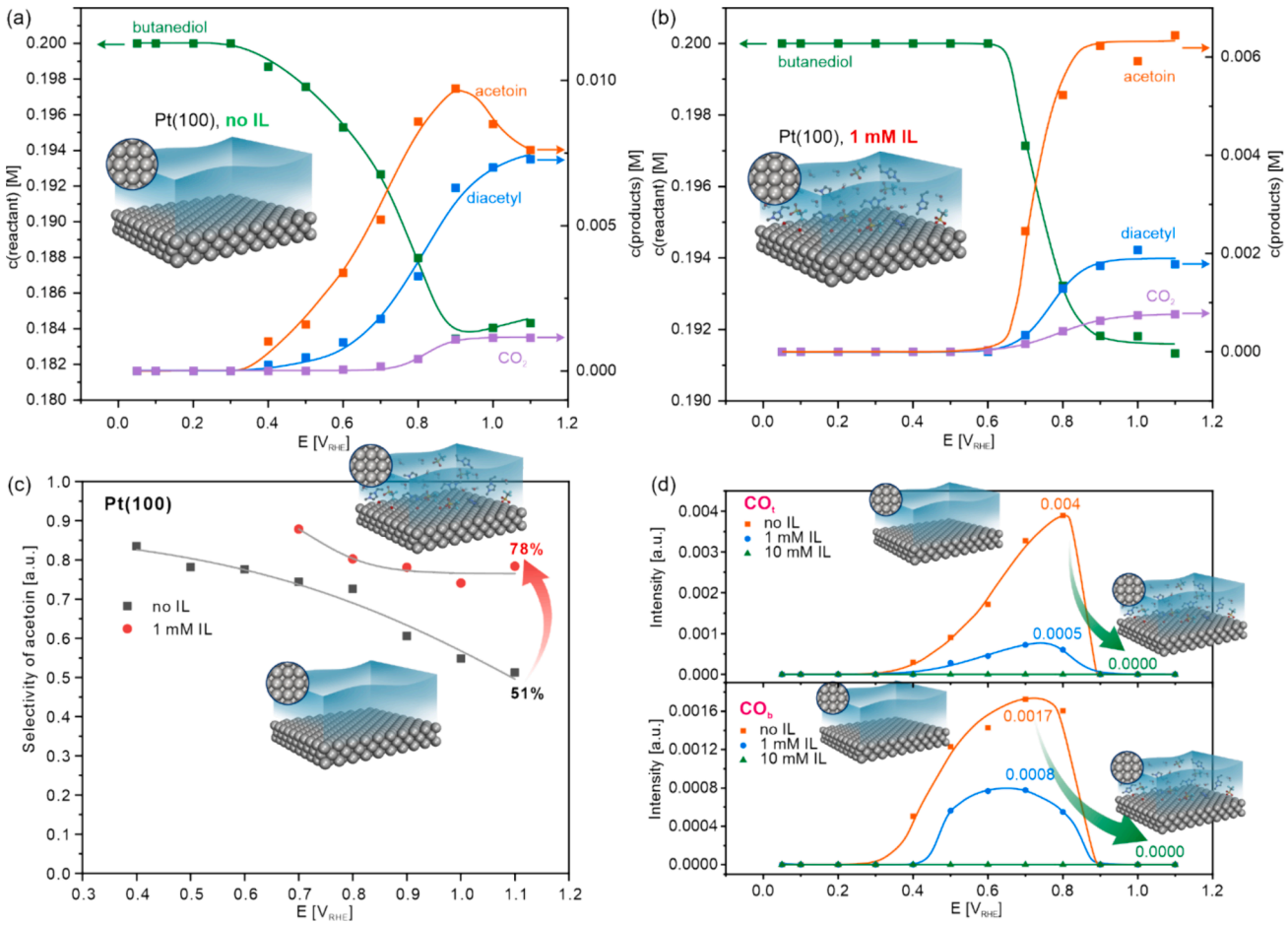

Fig. 5. Effect of low concentrations of the IL $[C_2C_1Im][OTf]$ on the activity, selectivity and CO formation during the oxidation of 2,3-butanediol on Pt(1 0 0); potential-dependent development of the concentrations of 2,3-butanediol (green), acetoin (orange), diacetyl (blue) and CO_2 (purple) in (a) the absence and (b) the presence of 1 mM IL; (c) effect of 1 mM IL on the selectivity to acetoin; (d) development of the band intensities of CO_t (top) and CO_b (bottom) in the absence and presence of different IL concentrations. (For interpretation of the references to colour in this figure legend, the reader is referred to the web version of this article.)

To complete the picture, we plotted the band intensities of the CO_t (Fig. 5d top) and CO_b (Fig. 5d bottom) bands in the absence (orange) and in the presence of the IL (1 mM: blue; 10 mM: green, determined from the spectra recorded with p-polarized light). Already at very low IL concentration (1 mM), the onset potential for CO formation shifts from 0.4 to 0.5 V_{RHE} and CO bands decrease in intensity as compared to the experiment without IL. Note that a direct correlation between band intensity and CO coverage is not possible due to coupling effects and different dynamic dipole moments [57]. At 10 mM, CO_{ads} formation is completely suppressed.

In previous work, we demonstrated that, in the presence of the IL $[C_2C_1Im][OTf]$, the $[OTf]^-$ anion adsorbs specifically on the Pt(1 1 1) surface in a potential-dependent and reversible manner, while we observed the cation in solution only [24,52]. Note that we cannot exclude statically adsorbed cations. In the presence of the IL, we observed a partial blocking of the OH_{ads} formation on the Pt surface [52]. We propose that this type of reversible adsorption also occurs on the Pt(1 0 0) surface and suggest that it is responsible for the increase of the onset potential of ketone formation and the lower activity due to partial blocking of the active sites. On the other hand, the adsorption of

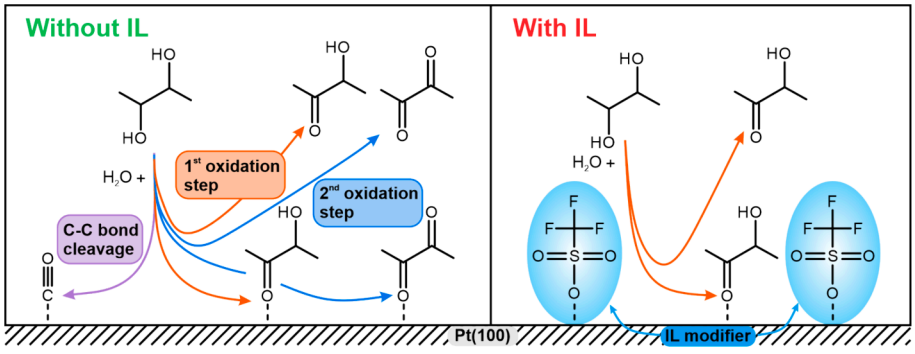

Scheme 2. Schematic representation of the processes occurring during the oxidation of 2,3-butanediol on the Pt(1 0 0) surface in the absence (left) and presence (right) of an IL modifier.

$[OTf]^-$ also leads to an increase of selectivity to acetoin and suppresses C—C bond cleavage and, as a result, CO formation (see Scheme 2). In our previous work, we proposed that for Pt(1 1 1) the potential-dependent adsorption of the $[OTf]^-$ anion suppresses the formation of surface OH especially in the potential window of the second oxidation step. Thus, the conversion of acetoin to diacetyl is prevented, increasing the selectivity towards acetoin [24]. In this work, we have also shown that there is an additional reaction channel, i.e. C—C bond cleavage that gives rise to formation of CO_{ads}. This channel is observed on Pt(1 0 0) terraces only. Once these (1 0 0) sites are modified by the IL, C—C bond cleavage is suppressed. Thus, the formation of CO, which is a poisoning species on the Pt catalysts, can be prevented. This finding is also relevant for Pt nanoparticles, which often expose a combination of (1 1 1), (1 0 0) and (1 1 0) facets and where the CO_{ads} can migrate between these facets.

4. Conclusions

In this work, we have studied the electrooxidation of 2,3-butanediol on the low index platinum surfaces Pt(1 1 1), Pt(1 0 0) and Pt(1 1 0) in acidic environment (0.1 M $HClO_4$) by EC-IRRAS. We elaborate the effect of the IL $[C_2C_1Im][OTf]$ on the activity, selectivity for the two products acetoin and diacetyl, and ability for C—C bond cleavage. From our results we conclude:

1. *Reaction products in solution*: All Pt(h k l) surfaces studied in this work are active for the electrooxidation of 2,3-butanediol. On all surfaces, partially oxidized acetoin and fully oxidized diacetyl are formed, with both products desorbing into the solution. However, the 2,3-butanediol electrooxidation is a structure sensitive reaction. Activity, selectivity and potential window for oxidation depend on the crystal facet. On Pt(1 1 1), the oxidation occurs in a potential window between 0.4 and 0.7 V_{RHE} and the potentials of the two sequential oxidation steps are well separated. On Pt(1 0 0) and Pt(1 1 0), the oxidation takes place in potential windows of 0.4 and 1.1 V_{RHE} and 0.5 and 0.9 V_{RHE}, respectively, and the two oxidation steps overlap. While the fully oxidized diacetyl is formed as the main product on Pt (1 1 1) and Pt(1 1 0), the selectivity towards the partially oxidized acetoin reaches ~50 % on the Pt(1 0 0) surface.
2. C—C *bond cleavage:* While all investigated surfaces are active for the oxidation of the secondary alcohol functionality, C—C bond cleavage occurs on Pt(1 0 0) sites only due to the ensemble effect. Adsorbed CO is formed as a reaction by-product, poisoning the surface.
3. *Effect of the IL on conversion, selectivity, and* C—C *bond cleavage on Pt (1 0 0)*: Even low concentrations of IL affect both activity and selectivity for the electrooxidation of 2,3-butanediol on Pt(1 0 0). While we observe a decrease in activity, the selectivity to the partially oxidized acetoin increases from about 50 % to almost 80 % in the presence of low concentration of the IL (1 mM $[C_2C_1Im][OTf]$). Most importantly, the IL suppresses C—C bond cleavage and, thus, prevents the formation of CO, which poisons the catalyst.
4. *Proposed mechanism:* We attribute the effects on conversion, selectivity, and C—C bond cleavage to the potential-dependent and reversible adsorption of the $[OTf]^-$ anion and additional interionic interactions. The specifically adsorbed $[OTf]^-$ blocks part of the surface sites, which leads to a decrease of activity. However, this adsorption also blocks OH formation in the potential window of the second oxidation step, which leads to an increase of selectivity for the partially oxidized acetoin. Finally, the adsorbate blocks the ensembles of Pt(1 0 0) terrace sites required for C—C bond cleavage, which suppresses the formation of CO.

Our work demonstrates the potential of ionic liquid modifiers for improving the selectivity of electrocatalysts. The IL not only affects the selectivity in a reaction system with two competing products (selective oxidation of different secondary alcohols), but also suppresses undesired side reactions (C—C bond cleavage). In a real electrocatalyst, the active particles will expose different facets and defect sites, which show different activity and interact differently with the IL. The pronounced structure dependence observed in this study shows that a detailed fundamental understanding will be required to design IL modified electrocatalysts for real applications.

Declaration of Generative AI and AI-assisted technologies in the writing process

During the preparation of this work the authors used DeepL in order to improve the language. After using this tool/service, the author(s) reviewed and edited the content as needed and take full responsibility for the content of the publication.

CRediT authorship contribution statement

Juntao Yang: Writing – original draft, Investigation, Data curation. **Florian Haßfurther:** Investigation, Writing – review & editing. **Felix Hilpert:** Investigation, Writing – review & editing. **Zarah Hussain:** Investigation, Writing – review & editing. **Tian Yang:** Writing – review & editing, Investigation. **Nicola Taccardi:** Writing – review & editing, Investigation. **Peter Wasserscheid:** Writing – review & editing, Supervision, Resources, Funding acquisition. **Olaf Brummel:** Writing – original draft, Supervision, Funding acquisition, Formal analysis, Conceptualization. **Jörg Libuda:** Writing – review & editing, Supervision, Resources, Funding acquisition, Conceptualization.

Declaration of competing interest

The authors declare that they have no known competing financial interests or personal relationships that could have appeared to influence the work reported in this paper.

Data availability

The data that support the findings of this study are presented in the Manuscript and the Supplementary Information. Source data are provided at Zenodo: https://doi.org/10.5281/zenodo.11004536.

Acknowledgements

The authors acknowledge financial support by the Deutsche Forschungsgemeinschaft (DFG) via Collaborative Research Centre SFB 1452 — Catalysis at Liquid Interfaces (project 431791331). Additional support is given by the Bavarian Ministry of Economic Affairs, Regional Development and Energy and the DFG via projects 431733372, and 453560721. We acknowledge the support from the China Scholarship Council (CSC) during the stay of J.Y. at the Friedrich-Alexander-Universität Erlangen-Nürnberg.

Appendix A. Supplementary material

Cyclic voltammograms of Pt(h k l) single crystal electrodes taken in the blank electrolyte, absence and presence of 2,3-butanediol. Comparison of the IR spectra of the 2,3-butanediol oxidation measured with p- and s-polarized light on Pt(h k l) single crystal electrodes; spectra are separated into CO and fingerprint regions; IR spectra of the 2,3-butanediol oxidation at different IL concentrations measured with s-polarized light; IR spectra of 2,3-butanediol oxidation on Pt(1 0 0) with and without Li(OTf). Supplementary data to this article can be found online at https://doi.org/10.1016/j.jcat.2024.115541.

References

[1] H. Mistry, A.S. Varela, S. Kühl, P. Strasser, B.R. Cuenya, Nanostructured electrocatalysts with tunable activity and selectivity, Nat. Rev. Mater. 1 (4) (2016) 16009, https://doi.org/10.1038/natrevmats.2016.9.

[2] U. Kernchen, B. Etzold, W. Korth, A. Jess, Solid catalyst ionic liquid layer (SCILL) - a new concept to improve selectivity illustrated by hydrogenation of cyclooctadiene, Chem. Eng. Technol. 30 (8) (2007) 985–994, https://doi.org/10.1002/ceat.200700050.

[3] J.D. Scholten, B.C. Leal, J. Dupont, Transition metal nanoparticle catalysis in ionic liquids, ACS Catal. 2 (1) (2012) 184–200, https://doi.org/10.1021/cs200525e.

[4] H.P. Steinrück, P. Wasserscheid, Ionic liquids in catalysis, Catal. Lett. 145 (1) (2015) 380–397, https://doi.org/10.1007/s10562-014-1435-x.

[5] J. Arras, E. Paki, C. Roth, J. Radnik, M. Lucas, P. Claus, How a supported metal is influenced by an ionic liquid: in-depth characterization of SCILL-type palladium catalysts and their hydrogen adsorption, J. Phys. Chem. C 114 (23) (2010) 10520–10526, https://doi.org/10.1021/jp1016196.

[6] M. Sobota, M. Happel, M. Amende, N. Paape, P. Wasserscheid, M. Laurin, J. Libuda, Ligand effects in SCILL model systems: site-specific interactions with Pt and Pd nanoparticles, Adv. Mater. 23 (22–23) (2011) 2617–2621, https://doi.org/10.1002/adma.201004064.

[7] J. Arras, M. Steffan, Y. Shayeghi, D. Ruppert, P. Claus, Regioselective catalytic hydrogenation of citral with ionic liquids as reaction modifiers, Green Chem. 11 (5) (2009) 716–772, https://doi.org/10.1039/b822992a.

[8] N. Szesni, A. Hagemeyer, F. Grossmann, R. Fischer, M. Urbancic, C. Lugmair, M. Sun, H.C. Hou, L. D. M. WO2013/057244A1, 2013.

[9] A.C. Garcia, T. Touzalin, C. Nieuwland, N. Perini, M.T.M. Koper, Oxygen evolution reaction enhancement of oxygen evolution activity of nickel oxyhydroxide by electrolyte alkali cations, Angew. Chemie - Int. Ed. 58 (2019) 12999–13003, https://doi.org/10.1002/anie.201905501.

[10] G.A. Kamat, J.A.Z. Zeledón, G.T.K.K. Gunasooriya, S.M. Dull, J.T. Perryman, J. K. Nørskov, M.B. Stevens, T.F. Jaramillo, Acid anion electrolyte effects on platinum for oxygen and hydrogen electrocatalysis Gaurav, Commnunications Chem. 5 (20) (2022), https://doi.org/10.1038/s42004-022-00635-1.

[11] A. So, W. Ju, T. Reier, P. Strasser, Tuning the catalytic activity and selectivity of Cu for CO_2 electroreduction in the presence of halides, ACS Catal. 6 (2016) 2136–2144, https://doi.org/10.1021/acscatal.5b02550.

[12] M. Galiński, A. Lewandowski, I. Stepniak, Ionic liquids as electrolytes, Electrochim. Acta 51 (26) (2006) 5567–5580, https://doi.org/10.1016/j.electacta.2006.03.016.

[13] G.R. Zhang, B.J.M. Etzold, Emerging applications of solid catalysts with ionic liquid layer concept in electrocatalysis, Adv. Funct. Mater. 31 (28) (2021), https://doi.org/10.1002/adfm.202010977.

[14] M. George, G.-R. Zhang, N. Schmitt, K. Brunnengräber, D.J.S. Sandbeck, K.J. J. Mayrhofer, S. Cherevko, B.J.M. Etzold, Effect of ionic liquid modification on the ORR performance and degradation mechanism of trimetallic PtNiMo/C catalysts, ACS Catal. 9 (9) (2019) 8682–8692, https://doi.org/10.1021/acscatal.9b01772.

[15] G.-R.-R. Zhang, T. Wolker, D.J.S.S. Sandbeck, M. Munoz, K.J.J.J. Mayrhofer, S. Cherevko, B.J.M.M. Etzold, Tuning the electrocatalytic performance of ionic liquid modified Pt catalysts for the oxygen reduction reaction via cationic chain engineering, ACS Catal. 8 (9) (2018) 8244–8254, https://doi.org/10.1021/acscatal.8b02018.

[16] G.R. Zhang, C. Yong, L.L. Shen, H. Yu, K. Brunnengräber, T. Imhof, D. Mei, B.J. M. Etzold, Increasing accessible active site density of non-precious metal oxygen reduction reaction catalysts through ionic liquid modification, ACS Appl. Mater. Interfaces 15 (15) (2023) 18781–18789, https://doi.org/10.1021/acsami.2c21441.

[17] T. Wolker, K. Brunnengräber, I. Martinaiou, N. Lorenz, G.R. Zhang, U.I. Kramm, B. J.M. Etzold, The effect of temperature on ionic liquid modified Fe-N-C catalysts for alkaline oxygen reduction reaction, J. Energy Chem. 68 (2022) 324–329, https://doi.org/10.1016/j.jechem.2021.11.042.

[18] G.R. Zhang, S.D. Straub, L.L. Shen, Y. Hermans, P. Schmatz, A.M. Reichert, J. P. Hofmann, I. Katsounaros, B.J.M.M. Etzold, Probing CO_2 reduction pathways for copper catalysis using an ionic liquid as a chemical trapping agent, Angew. Chemie - Int. Ed. 59 (41) (2020) 18095–18102, https://doi.org/10.1002/anie.202009498.

[19] Y. Li, J. Hart, L. Profitt, S. Intikhab, S. Chatterjee, M. Taheri, J. Snyder, Sequential capacitive deposition of ionic liquids for conformal thin film coatings on oxygen reduction reaction electrocatalysts, ACS Catal. (2019) 9311–9316, https://doi.org/10.1021/acscatal.9b03157.

[20] S. Favero, I.E.L. Stephens, M.M. Titirici, Engineering the electrochemical interface of oxygen reduction electrocatalysts with ionic liquids: a review, Adv. Energy Sustain. Res. 2 (1) (2021), https://doi.org/10.1002/aesr.202000062.

[21] G.R. Zhang, B.J.M. Etzold, Ionic liquids in electrocatalysis, J. Energy Chem. 25 (2) (2016) 199–207, https://doi.org/10.1016/j.jechem.2016.01.007.

[22] J. Snyder, T. Fujita, M.W. Chen, J. Erlebacher, Oxygen reduction in nanoporous metal-ionic liquid composite electrocatalysts, Nat. Mater. 9 (11) (2010) 904–907, https://doi.org/10.1038/nmat2878.

[23] J. Snyder, K. Livi, J. Erlebacher, Oxygen reduction reaction performance of [MTBD][Beti]-encapsulated nanoporous NiPt alloy nanoparticles, Adv. Funct. Mater. 23 (44) (2013) 5494–5501, https://doi.org/10.1002/adfm.201301144.

[24] T. Yang, J. Yang, X. Deng, E. Franz, L. Fromm, N. Taccardi, Z. Liu, A. Görling, P. Wasserscheid, O. Brummel, J. Libuda, Modifying the electrocatalytic selectivity of oxidation reactions with ionic liquids, Angew. Chemie Int. Ed. (2022) 1–6, https://doi.org/10.1002/anie.202202957.

[25] M. Kastenmeier, E. Franz, F. Waidhas, T. Yang, N. Taccardi, P. Wasserscheid, Competition of acetone reduction and hydrogen evolution on Pt single crystal electrodes in the absence and presence of the ionic liquid $[C_2C_1Im][OTf]$, 2023, doi: 10.1021/acs.jpcc.3c06260.

[26] K. Brunnengräber, K. Jeschonek, M. George, G. Zhang, B.J.M. Etzold, Ionic liquid modified electrocatalysts: a STEM-EDX approach for identification of local distributions within ionomer containing catalysts layers, Chemistry-Methods 3 (8) (2023), https://doi.org/10.1002/cmtd.202200084.

[27] G.R. Zhang, M. Munoz, B.J.M. Etzold, Boosting performance of low temperature fuel cell catalysts by subtle ionic liquid modification, ACS Appl. Mater. Interfaces 7 (6) (2015) 3562–3570, https://doi.org/10.1021/am5074003.

[28] J.S. Lee, T. Lee, H.K. Song, J. Cho, B.S. Kim, Ionic Liquid modified graphene nanosheets anchoring manganese oxide nanoparticles as efficient electrocatalysts for Zn-air batteries, Energ. Environ. Sci. 4 (10) (2011) 4148–4154, https://doi.org/10.1039/c1ee01942b.

[29] M. Qiao, C. Tang, L.C. Tanase, C.M. Teodorescu, C. Chen, Q. Zhang, M.M. Titirici, Oxygenophilic ionic liquids promote the oxygen reduction reaction in Pt-free carbon electrocatalysts, Mater. Horizons 4 (5) (2017) 895–899, https://doi.org/10.1039/c7mh00298j.

[30] Y. Tan, C. Xu, G. Chen, N. Zheng, Q. Xie, A graphene-platinum nanoparticles-ionic liquid composite catalyst for methanol-tolerant oxygen reduction reaction, Energ. Environ. Sci. 5 (5) (2012) 6923–6927, https://doi.org/10.1039/c2ee21411c.

[31] H. Zhang, J. Liang, B. Xia, Y. Li, S. Du, Ionic liquid modified Pt/C electrocatalysts for cathode application in proton exchange membrane fuel cells, Front. Chem. Sci. Eng. 13 (4) (2019) 695–701, https://doi.org/10.1007/s11705-019-1838-8.

[32] D.S. Silvester, L. Aldous, C. Hardacre, R.G. Compton, An electrochemical study of the oxidation of hydrogen at platinum electrodes in several room temperature ionic liquids, J. Phys. Chem. B 111 (18) (2007) 5000–5007, https://doi.org/10.1021/jp067236v.

[33] S. Ji, T. Li, Z. Gao, Y.Y. Song, J.J. Xu, Boosting the oxygen evolution reaction performance of CoS_2 microspheres by subtle ionic liquid modification, Chem. Commun. 54 (63) (2018) 8765–8768, https://doi.org/10.1039/c8cc05352a.

[34] T.N. Pham Truong, H. Randriamahazaka, J. Ghilane, Polymer brushes ionic liquid as a catalyst for oxygen reduction and oxygen evolution reactions, ACS Catal. 8 (2) (2018) 869–875, https://doi.org/10.1021/acscatal.7b03158.

[35] Q. Wang, Y. Gao, Z. Ma, Y. Zhang, W. Ni, H.A. Younus, C. Zhang, Z. Chen, S. Zhang, Supported Ionic liquid phase-boosted highly active and durable electrocatalysts towards hydrogen evolution reaction in acidic electrolyte, J. Energy Chem. 54 (2021) 342–351, https://doi.org/10.1016/j.jechem.2020.06.012.

[36] G. Iijima, T. Kitagawa, A. Katayama, T. Inomata, H. Yamaguchi, K. Suzuki, K. Hirata, Y. Hijikata, M. Ito, H. Masuda, CO_2 reduction promoted by imidazole supported on a phosphonium-type ionic-liquid-modified Au electrode at a low overpotential, ACS Catal. 8 (3) (2018) 1990–2000, https://doi.org/10.1021/acscatal.7b03274.

[37] P. Tamilarasan, S. Ramaprabhu, A polymerized ionic liquid functionalized cathode catalyst support for a proton exchange membrane CO_2 conversion cell, RSC Adv. 5 (32) (2015) 24864–24871, https://doi.org/10.1039/c5ra03002a.

[38] K. Huang, T. Song, O. Morales-Collazo, H. Jia, J.F. Brennecke, Enhancing Pt/C catalysts for the oxygen reduction reaction with protic ionic liquids: the effect of anion structure, J. Electrochem. Soc. 164 (13) (2017) F1448–F1459, https://doi.org/10.1149/2.1071713jes.

[39] F. Luo, Q. Zhang, Z. Yang, L. Guo, X. Yu, K. Qu, Y. Ling, J. Yang, W. Cai, Fabrication of stable and well-connected proton path in catalyst layer for high temperature polymer electrolyte fuel cells, ChemCatChem 10 (22) (2018) 5314–5322, https://doi.org/10.1002/cctc.201801256.

[40] A. Hilmi, M. Dupont, E.M. Belgsir, J.M. Léger, C. Lamy, Electrocatalytic oxidation of aliphatic diols in acid medium. III. Structural effects during the oxidation of 2,3-butanediol stereoisomers at platinum single crystal electrodes, J. Electroanal. Chem. 376 (1–2) (1994) 161–166, https://doi.org/10.1016/0022-0728(94)03596-2.

[41] A. Kuhn, F.C. Anson, Effects of chirality during electrochemical oxidation of 2,3 butanediol stereoisomers, J. Electroanal. Chem. 410 (2) (1996) 243–246, https://doi.org/10.1016/0022-0728(96)04676-1.

[42] A. Hilmi, E.M. Belgsir, J.M. Léger, C. Lamy, Electrocatalytic oxidation of aliphatic diols part V. Electro-oxidation of butanediols on platinum based electrodes, J. Electroanal. Chem. 435 (1–2) (1997) 69–75, https://doi.org/10.1016/S0022-0728(97)00007-7.

[43] B.M. Choudary, M. Lakshmi Kantam, P. Lakshmi Santhi, New and ecofriendly options for the production of speciality and fine chemicals, Catal. Today 57 (1–2) (2000) 17–32, https://doi.org/10.1016/S0920-5861(99)00307-7.

[44] I. Nadal, J. Rico, G. Pérez-Martínez, M.J. Yebra, V. Monedero, Diacetyl and acetoin production from whey permeate using engineered Lactobacillus casei, J. Ind. Microbiol. Biotechnol. 36 (9) (2009) 1233–1237, https://doi.org/10.1007/s10295-009-0617-9.

[45] H. Tian, B. Yu, H. Yu, C. Chen, Evaluation of the synergistic olfactory effects of diacetyl, acetaldehyde, and acetoin in a yogurt matrix using odor threshold, aroma intensity, and electronic nose analyses, J. Dairy Sci. 103 (9) (2020) 7957–7967, https://doi.org/10.3168/jds.2019-17495.

[46] F.Z. Hegazi, I.G. Abo-Elnaga, Production of acetoin and diacetyl by lactic acid bacteria in skimmed milk with added citrate and pyruvate, Z. Lebensm. Unters. Forsch. 171 (5) (1980) 367–370, https://doi.org/10.1007/BF01087136.

[47] K. Müller, S. Thiele, P. Wasserscheid, Evaluations of concepts for the integration of fuel cells in liquid organic hydrogen carrier systems, Energy Fuel 33 (10) (2019) 10324–10330, https://doi.org/10.1021/acs.energyfuels.9b01939.

[48] M. Brodt, K. Müller, J. Kerres, I. Katsounaros, K. Mayrhofer, P. Preuster, P. Wasserscheid, S. Thiele, The 2-propanol fuel cell: a review from the perspective of a hydrogen energy economy, Energy Technol. 9 (9) (2021), https://doi.org/10.1002/ente.202100164.

[49] J. Cho, B. Kim, S. Venkateshalu, D.Y. Chung, K. Lee, S.I. Choi, Electrochemically activatable liquid organic hydrogen carriers and their applications, J. Am. Chem. Soc. 145 (31) (2023) 16951–16965, https://doi.org/10.1021/jacs.2c13324.
[50] G. Sievi, D. Geburtig, T. Skeledzic, A. Bösmann, P. Preuster, O. Brummel, F. Waidhas, M.A. Montero, P. Khanipour, I. Katsounaros, J. Libuda, K.J. J. Mayrhofer, P. Wasserscheid, Towards an efficient liquid organic hydrogen carrier fuel cell concept, Energ. Environ. Sci. 12 (7) (2019) 2305–2314, https://doi.org/10.1039/c9ee01324e.
[51] D.S. Mekazni, R.M. Arán-Ais, E. Herrero, J.M. Feliu, On the oxidation of isopropanol on platinum single crystal electrodes. A detailed voltammetric and FTIR study, J. Power Sources 556 (September 2022) (2023), https://doi.org/10.1016/j.jpowsour.2022.232396.
[52] O. Brummel, F. Faisal, T. Bauer, K. Pohako-Esko, P. Wasserscheid, J. Libuda, Ionic liquid-modified electrocatalysts: the interaction of $[C_1C_2Im][OTf]$ with Pt(111) and its influence on methanol oxidation studied by electrochemical IR spectroscopy, Electrochim. Acta 188 (2016) 825–836, https://doi.org/10.1016/j.electacta.2015.12.006.
[53] F. Faisal, M. Bertram, C. Stumm, F. Waidhas, O. Brummel, J. Libuda, Preparation of complex model electrocatalysts in ultra-high vacuum and transfer into the electrolyte for electrochemical IR spectroscopy and other techniques, Rev. Sci. Instrum. 89 (11) (2018), https://doi.org/10.1063/1.5047056.
[54] J. Clavilier, The role of anion on the electrochemical behaviour of a 111 platinum surface; an unusual splitting of the voltammogram in the hydrogen region, J. Electroanal. Chem. Interfacial Electrochem. 107 (1) (1980) 211–216.
[55] C. Korzeniewski, V. Climent, J.M. Feliu, Electrochemistry at platinum single crystal electrodes, Electroanal. Chem. Ser. Adv. 24 (2011) 75–170, https://doi.org/10.1201/b11480-3.
[56] T. Iwasita, F.C. Nart, In situ infrared spectroscopy at electrochemical interfaces, Prog. Surf. Sci. 55 (4) (1997) 271–340, https://doi.org/10.1016/S0079-6816(97)00032-4.
[57] I. Villegas, M.J. Weaver, Carbon monoxide adlayer structures on platinum (111) electrodes: a synergy between in-situ scanning tunneling microscopy and infrared, Spectroscopy 101 (2) (1994) 1648–1660.
[58] O. Brummel, L. Jacobse, A. Simanenko, X. Deng, S. Geile, O. Gutowski, V. Vonk, Y. Lykhach, A. Stierle, J. Libuda, Chemical and structural in-situ characterization of model electrocatalysts by combined infrared spectroscopy and surface X-ray diffraction, J. Phys. Chem. Lett. 14 (39) (2023) 8820–8827, https://doi.org/10.1021/acs.jpclett.3c01777.
[59] F. Hoffmann, Infrared reflection-absorption spectroscopy of adsorbed molecules, Surf. Sci. Rep. 3 (2–3) (1983) 107, https://doi.org/10.1016/0167-5729(83)90001-8.
[60] F.J. Vidal-Iglesias, J. Solla-Gullón, V. Montiel, J.M. Feliu, A. Aldaz, Ammonia selective oxidation on Pt (100) sites in an alkaline medium, J. Phys. Chem. B 109 (2005) 12914–12919.
[61] F. Calle-vallejo, M.T.M. Koper, Theoretical considerations on the electroreduction of CO to C_2 species on Cu (100) electrodes, Angew. Chemie - Int. Ed. 52 (2013) 7282–7285, https://doi.org/10.1002/anie.201301470.
[62] K.J.P. Schouten, Z. Qin, M.T.M. Koper, Two pathways for the formation of ethylene in CO reduction on single-crystal copper electrodes, J. Am. Chem. Soc. 134 (2012) 9864–9867, https://doi.org/10.1021/ja302668n.
[63] S. Strbac, R.R. Ad, The influence of OH chemisorption on the catalytic properties of gold single crystal surfaces for oxygen reduction in alkaline solutions, J. Electroanal. Chem. 403 (1996) 169–181.
[64] O.A. Hazzazi, S.E. Huxter, R. Taylor, B. Palmer, L. Gilbert, G.A. Attard, Electrochemical studies of irreversibly adsorbed ethyl pyruvate on Pt hkl and epitaxial Pd/Pt hkl adlayers, J. Electroanal. Chem. 640 (1–2) (2010) 8–16, https://doi.org/10.1016/j.jelechem.2009.12.026.
[65] C.J. Bondue, Z. Liang, M.T.M. Koper, Dissociative adsorption of acetone on platinum single-crystal electrodes, J. Phys. Chem. C 125 (12) (2021) 6643–6649, https://doi.org/10.1021/acs.jpcc.0c11360.
[66] H. Li, F. Calle-Vallejo, M.J. Kolb, Y. Kwon, Y. Li, M.T.M. Koper, Why (100) terraces break and make bonds: oxidation of dimethyl ether on platinum single-crystal electrodes, J. Am. Chem. Soc. 135 (2013) 14329–14338.
[67] H. Li, Y. Li, M.T.M. Koper, F. Calle-Vallejo, Bond-making and breaking between carbon, nitrogen, and oxygen in electrocatalysis, J. Am. Chem. Soc. 136 (2014) 15694–15701.
[68] F. Waidhas, S. Haschke, P. Khanipour, L. Fromm, A. Görling, J. Bachmann, I. Katsounaros, K.J.J. Mayrhofer, O. Brummel, J. Libuda, Secondary alcohols as rechargeable electrofuels: electrooxidation of isopropyl alcohol at Pt electrodes, ACS Catal. 10 (12) (2020) 6831–6842, https://doi.org/10.1021/acscatal.0c00818.
[69] T. Yang, M. Kastenmeier, M. Ronovský, L. Fusek, T. Skála, F. Waidhas, M. Bertram, N. Tsud, P. Matvija, K.C. Prince, V. Matolín, Z. Liu, V. Johánek, J. Mysliveček, Y. Lykhach, O. Brummel, J. Libuda, Selective electrooxidation of 2-propanol on Pt nanoparticles supported on Co_3O_4: an in-situ study on atomically defined model systems, J. Phys. D: Appl. Phys. 54 (16) (2021), https://doi.org/10.1088/1361-6463/abd9ea.
[70] I. Mangoufis-Giasin, L. Fusek, T. Yang, P. Khanipour, O. Brummel, J. Libuda, K.J. J. Mayrhofer, F. Calle-Vallejo, I. Katsounaros, Activity trends for the selective oxidation of 2-propanol to acetone on noble metal electrodes in alkaline electrolyte, ACS Catal. 13 (22) (2023) 14562–14569, https://doi.org/10.1021/acscatal.3c03423.